CFD-DEM MODELING OF PARTICLE COATING IN A PRISMATIC SPOUTED BED AND IMPROVEMENT OF SPOUTING STABILITY

Swantje Pietsch[1*], Paul Kieckhefen[1], Stefan Heinrich[1], Michael Müller[2], Michael Schönherr[2], Frank Kleine Jäger[2]

[1]*Hamburg University of Technology, Institute of Solids Process Engineering and Particle Technology, Denickestraße 15, 21073 Hamburg, Germany*

[2] *BASF SE, GCP/TT, 67056 Ludwigshafen, Germany*

**Email: swantje.pietsch@tuhh.de*

Abstract – In this contribution coupled CFD-DEM simulations of a three-dimensional prismatic spouted bed for coating purposes were performed. The simulations were validated by means of pressure drop fluctuations and flow pattern with respect to experimental data. In order to increase the spouting stability, draft plates were inserted into the process chamber. To investigate the influence of flow stability on coating quality, droplets were injected in a post-processing step and deposited on colliding particle parcels. By means of that tool the time-dependent cumulative distribution function of the particle liquid loading was calculated and compared for different process configurations.

1. INTRODUCTION

1.1. Spouted bed technology

Since its invention in 1954 by Mathur and Gishler [1], spouted bed technology has been applied in a wide range of applications as e.g. granulation and coating, combustion and drying. In contrast to the conventional fluidized bed, the fluidization gas enters the process chamber of the spouted bed via a tube or slits. At low gas velocities, the bed remains static, which is called the fixed bed regime. By slightly increasing the velocity bubbles are formed, which are transported to the bed surface. After reaching the so-called minimum spouting velocity, particles are accelerated by the high velocity in the gas inlet region and the spout is formed. Due to the increasing cross-sectional area of the process chamber, the particle velocity is reduced with increasing height. At the highest point, the so-called fountain region, the direction of particle movement changes and the particles fall along the apparatus' walls back into the annulus zone, which is the area with highest particle concentration. Generally, three geometry configurations of spouted beds can be distinguished: axisymmetric, asymmetric and slot-rectangular spouted beds. Latter have the advantage of scale-up possibility in depth, whereby difficulties have been reported due to three-dimensional effects and changings in flow pattern [2]. Besides the geometry of the apparatus, (i) the particle bed height, (ii) the material properties and the (iii) gas velocity have an influence on the spouting stability [3]. The apparatus investigated in this work can be assigned to the family of slot-rectangular beds and is often termed as prismatic spouted bed since the used static bed height is usually lower than the prismatic region of the apparatus. A pseudo two-dimensional version of a prismatic spouted bed was experimentally and numerically investigated by Salikov et al. [4]. By analysis of the pressure drop signal they obtained a regime map for their investigated apparatus and bed material showing different regions of stable and instable spouting. After reaching the minimum spouting velocity a region of dense stable spouting could be observed. With increasing gas velocity the instable regime was reached, which is defined by lateral spout deflections and variations in bed expansion. At higher gas velocities, a second stable region, the dilute spouting regime with lower particle void fractions than in the dense region, was observed. By inserting draft plates into the process chamber, the region of dense stable spouting could be significantly increased [5]. Besides Salikov et al. other research groups used pressure drop signal analysis to quantify the flow stability in spouted beds. Freitas et al. [6], Chen et al. [3], Piskova and Mörl [7] and others used a Fast Fourier Transform of the pressure drop fluctuations to find stable spouting regimes in slot-rectangular spouted beds. Gryczka et al. [8] investigated a prismatic spouted bed. By means of the FFT power plot they found the dominant frequency of the pressure drop fluctuations as a characteristic value of stable spouting to be about 6 Hz for Geldart D systems. Van den Bleek and Schouten [9] and Salikov et al. [4] also used approaches of the deterministic chaos theory to characterize the spouting stability by means of the self-similarity pressure fluctuations of fluidized or spouted beds, respectively.

1.2. Numerical investigations

Due to the complex granular dynamics and a lack of empirical correlations for scale-up or configuration changes, numerical simulation of gas-solid processes has become more and more important. With today's high performance clusters, millions of particles can be modeled which allows in combination with coarse-graining methods the investigation of processes of industrial scale. Generally, two main modeling approaches can be distinguished: Euler-Euler and Euler-Lagrange methods. In Euler-Euler simulations both the fluid and the granular phase are treated as continua. One prominent approach of Euler-Euler simulations is the Two-Fluid-Model (TFM) which uses the Kinetic Theory of Granular Flow (KTGF) [10]. Two-Fluid-Models are solved on a numerical grid, whereby the particles' motions and contacts are not resolved but handled by statistics and closure laws. In Euler-Lagrange simulations the fluid flow is solved on a numerical grid and each individual particle is tracked. The tracking of the particles and its contact forces is an important advantage compared to Euler-Euler simulations because it allows the analysis of bed dynamics on the scale of single particles and opens access to information that are difficult to obtain from experiments as e.g. collision frequencies, trajectories or rotational velocities. One of the most frequently applied approaches is the CFD-DEM simulation approach. Computational Fluid Dynamics (CFD) describes the fluid phase by solving the Navier Stokes equations with different discretization approaches available. The motion and forces of particles are determined by Newton's equations of motion via Discrete Element Method (DEM). In recent years, plenty of work has been done in the area of CFD-DEM simulations of fluidized and spouted beds. Nevertheless, most of the research focused on axisymmetric spouted beds or on pseudo two-dimensional apparatuses in order to reduce the computational effort. Recently Sutkar et al. [11] investigated a pseudo two-dimensional spout fluidized bed with liquid injection via CFD-DEM simulations. In their approach the droplets' motion is as well as the particles' motion described by DEM. During a collision of particle and droplet, mass, volume and momentum are transferred to the particle which results in a particle mass, volume and momentum increase. Simulation results were verified by analytical solutions and flow pattern, velocities and pressure drop showed fair agreement with experiments of visual observations and an infrared thermography.

The aim of this work was the experimental and numerical investigation of a three-dimensional prismatic spouted bed used for coating purposes. The spouting stability was quantified by means of Fourier transformation of the pressure drop signal. Draft plates were inserted into the process chamber to increase the range of stable spouting. By experimental investigations the spray pattern of the used nozzle was determined and this area was used to create the simulation mesh around the nozzle. Droplets were injected in post-processing step and contacts between droplets and particle parcels were determined. By means of that the time dependent particle liquid loading was analyzed for different gas volume flow rates. Additionally, the influence of the draft plates on the liquid injection was investigated.

2. MATERIAL AND METHODS

The investigated spouted bed was the commercial ProCell 5 plant (Glatt, Germany) as shown in Fig. 1.

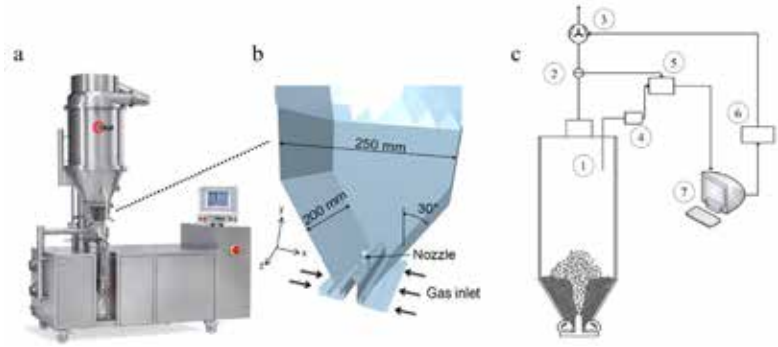

Fig. 1: ProCell 5 (Glatt, Germany): (a) Laboratory plant, (b) Geometry of the process chamber with nozzle in bottom-spray configuration, (c) Flow chart of the experimental setup of transparent ProCell 5 process chamber: 1) apparatus, 2) anemometer, 3) fan, 4) high speed pressure detector, 5) analogue-to-digital converter, 6) frequency converter, 7) computer.

Due to the small size of the inserted view window, a transparent replica of the process chamber (Fig. 1c) was installed to visually observe the flow pattern in cases without liquid injection and for high frequency pressure drop measurements. The process chamber is made off Plexiglas and has the same geometry as original Glatt ProCell 5 chamber. A high speed video camera was positioned in front of the chamber to record the particle flow pattern. Air is sucked through the apparatuses by an exhaust fan so that the processes are operated at under-pressure conditions. The air enters the process chambers through two horizontal parallel gas inlet slits with a maximum height of 3.5 mm. By reducing the height of the slits via movable cylinders, the gas velocity can be adjusted during the process which allows the breakage of local plugging without a need for stopping the process. In the transparent replica, the pressure drop is measured in the freeboard above the particle bed with a high-speed differential pressure detector (PD-23/8666.1, Keller, Germany). The sensor is connected to a signal converter and a data acquisition system as shown in Fig. 1. The pressure is recorded with a sampling frequency of 400 Hz in the experiments and with 1 kHz in the simulations. Experiments with liquid injection were performed in the original Glatt apparatus where a two-fluid nozzle was installed in bottom-spray configuration. In order to trace the particle coating and to determine the spray pattern, a dye was added to the water-based suspension. Nearly monodisperse spherical γ-Al_2O_3 particles (Sasol, Germany) with a mean diameter of 656 µm were used. In the simulations, ideally monosized spherical particles were assumed. A bed filling of 1 kg was used and gas volume flow rates of 70, 100 and 120 m³/h were chosen. Simulations were performed for 13 seconds whereby only the last ten seconds were used for analysis in order to exclude start-up effects.

3. SIMULATIONS

3.1. Numerical model

CFD-DEM simulations were performed with open source software CFDEMcoupling that couples CFD tool OpenFOAM with DEM software LIGGGHTS. The geometry of the process chamber shown in Fig. 1b was implemented and the simulation mesh was generated with OpenFOAM meshing tool *snappyHexMesh*. In order to capture the fine inlet geometry a grid size of 3.125 mm was chosen, whereas the main part of the process chamber had a cell size of 6.25 mm and in the upper part above a height of 0.5 m a grid size of 12.5 mm was used as there are almost no particles in that region. The mesh around the nozzle was generated according to the experimental determined spray pattern, as described in 4.2. In total, the mesh comprised around 700,000 cells of mostly hexahedral type.

The gas phase dynamics in presence of an additional granular phase were solved by applying the PISO algorithm in OpenFOAM to the incompressible Navier-Stokes equations:

$$\frac{\partial \alpha_f}{\partial t} + \nabla \cdot \left(\alpha_f \boldsymbol{u}_f\right) = 0 \tag{1}$$

$$\frac{\partial (\alpha_f \boldsymbol{u}_f)}{\partial t} + \nabla \cdot \left(\alpha_f \boldsymbol{u}_f \boldsymbol{u}_f\right) = -\frac{\alpha_f}{\rho_f}\nabla p - \frac{1}{\rho_f}\boldsymbol{R}_{pf} + \nabla \cdot \left(\frac{\alpha_f}{\rho_f}\boldsymbol{\tau}\right), \tag{2}$$

where p is the pressure, $\boldsymbol{g}$ is the gravitational constant, α_f is the volume fraction of the fluid, $\boldsymbol{u}_f$ is its velocity and ρ_f its density. The stress tensor $\boldsymbol{\tau}$ can be calculated via $\boldsymbol{\tau} = \mu_f \nabla \boldsymbol{u}_f$, where μ_f is the dynamic viscosity of the fluid. The term $\boldsymbol{R}_{pf}$ represents the momentum exchange between the fluid and the granular phase and is for numerical reasons split-up into an implicit and an explicit term using the averaged particle velocity $\boldsymbol{u}_p$ in the regarded cell.

$$\boldsymbol{R}_{pf} = K_{pf}\left(\boldsymbol{u}_f - \langle \boldsymbol{u}_p \rangle\right) \tag{3}$$

The momentum exchange coefficient K_{pf} contains the drag forces $\boldsymbol{F}_d$ that are acting in the regarded cell volume V_{cell}.

$$K_{pf} = \frac{\alpha_f \cdot |\sum_i \boldsymbol{F}_d|}{V_{cell}|\boldsymbol{u}_f - \langle \boldsymbol{u}_p \rangle|} \tag{4}$$

K_{pf} can be calculated with different drag models. Most of these models are of empirical or half-empirical nature. In this contribution, the drag model by Beetstra et al. [12] was used as it had shown high physical consistency with experiments in former investigations. The fluid velocity field is transferred to DEM which determines the interactions, velocities and forces of the particles by solving Newton's equations of motion:

$$m_i \ddot{\boldsymbol{x}}_i = \sum_i \boldsymbol{F}_i \tag{5}$$

$$I_i \dot{\boldsymbol{\omega}}_i = \sum_i \boldsymbol{M}_i \tag{6}$$

with masses m_i, center of mass positions $\boldsymbol{x}_i$, forces $\boldsymbol{F}_i$, inertia tensors I_i, angular velocities $\boldsymbol{\omega}_i$ and torques $\boldsymbol{M}_i$. The DEM calculations are carried out until the time step of CFD, which is usually bigger than the one of DEM, is reached. If that is the case, the simulation run time is updated and after checking that it is still below the end time, the procedure starts again whereby the Navier-Stokes equations are now fed with the new particle forces and velocities. A detailed description of the CFD-DEM coupling procedure can be found in e.g. the work of Deen et al. [13]. The particle collisions were modeled by a soft-sphere model based on the correlations of Hertz [14]. Even though the computational power is continuously increasing, coarse-graining methods are necessary to model processes on an industrial or, in case of fine particles, even on a laboratory scale. In this contribution the coarse-graining approach according to Bierwisch et al. [15] was used. In this apporach, several particles are represented by parcels. In order to preserve energy density and energy evolution during scaling, dimensionless numbers have to be kept constant as well as the collision properties such as the restitution coefficient. The liquid injection was performed in this contribution after the resource-intensive simulations. The post-processing-solver, which is based on a combination of the *sprayFoam*-solver and the *cfdemPostproc*-post-processing tool, loads the velocity fields and particle positions. A Lagrangian droplet phase is allowed to evolve in the loaded velocity fields. Droplets were injected with a frequency of $2.5 \cdot 10^6$ s^{-1} at the nozzle inlet patch with a mass flow rate of 5 g/min. A particle-droplet capturing efficiency of 100% was assumed. No evaporation was modeled meaning that the liquid stayed as a layer around the particle. In the time loop of the solver, droplet cloud evolution was alternated with deposition steps, in which contact detection was performed and droplets were captured by the particles.

3.2. Simulation setup

The particle properties were measured in several experimental setups. For example, the coefficient of restitution was determined in a free-fall device, as described in [16] and Young's modulus was measured with TextureAnalyzer (Stable Micro Systems, UK). The fluid and particle properties and the used simulation parameters are given in Table 1. As an implicit solver was used, the CFD time step Δt_{CFD} of $5 \cdot 10^{-5}$ s yielded regardless of Courant-Numbers of $\mathrm{Co} = \max \frac{\mathrm{U}\,\Delta t_{CFD}}{\Delta x} < 3$ stable simulations. The DEM time step was set to be about 20 % of the Rayleigh time. As CFD-DEM coupling interval and as the post-processing coupling interval between particles and liquid parcels the CFD time step was used.

Table 1: Fluid and particle properties and simulation parameters.

PARAMETER/SETTING	VALUE	UNIT	PARAMETER/SETTING	VALUE	UNIT
Slit height h	3.5	mm	Wall:		
Time step:			- Young's modulus Y_w	2.5	GPa
- CFD Δt_{CFD}	$5 \cdot 10^{-5}$	s	- Poisson ratio ϑ_w	0.3	-
- DEM Δt_{DEM}	$2.5 \cdot 10^{-7}$	s	Restitution coefficient:		
- Liquid injection Δt_{post}	10^{-4}	s	Particle-particle e_{p-p}	0.72	-
Particle diameter d_p	656	µm	Particle-wall e_{p-w}	0.73	-
Scaling factor δ	4	-	Static friction:		
Particle density ρ_p	1328	kg/m³	- Particle-particle $\mu_{s,\,p-p}$	0.06	-
Fluid density ρ_f	1.225	kg/m³	- Particle-wall $\mu_{s,\,p-w}$	0.05	-
Fluid dynamic viscosity μ_f	$1.7894 \cdot 10^{-5}$	kg/(m·s)	Field sampling frequency	10^4	Hz
Particles:			Liquid injection:		
- Young's modulus Y_p	3.06	GPa	- Parcel injection rate	10^5	Hz
- Poisson ratio ϑ_p	0.3	-	- Mass rate	5	g/min

3.3. Analysis of particle surface coverages

For analyzing the surface coverage, a simple statistical approach [17] based on the surface coverage due to the impact of a single droplet in relation to the total surface of a particle parcel is as follows:

$$\frac{\mathrm{S_{p,covered}}}{\mathrm{S_p}} = 1 - \left(1 - \eta_{\mathrm{coverage}} \frac{\mathrm{A_{droplet,proj}}}{\mathrm{S_p}}\right)^{\mathrm{N_{impacts}}} \tag{7}$$

where $S_p = \pi d_p^2 \delta^2$ is the parcel surface, $A_{droplet,proj} = \frac{\pi}{4} d_d^2$ is the projected surface of a single droplet, $N_{impacts} = \frac{m_{deposited\ liquid}}{m_{droplet}}$ is the number of impact events and $\eta_{coverage}$ is the coverage efficiency of a single impact regarding the affected area, in this case assumed to be 1 for simplicity.

3.4. Fourier transformation

For analysis of the spouting stability and for validation purposes, the measured gas pressure fluctuations were analyzed by using Fourier transformation $\mathcal{F}$ in the Python package *numpy*. The transformation decomposes the original function into sinusoids of different frequencies with their respective amplitudes. In this work, the transformation of the time dependent pressure signal $p(t_m)$ is defined as follows [18]:

$$\mathcal{F}p(t)(\omega_k) = \frac{1}{N_{data\ points}} \sum_{m=0}^{N_{datapoints}-1} p(t_m) e^{-\frac{2\pi m k}{N_{datapoints}}} \quad (8)$$

where $N_{data\ points}$ is the number of sampling points and ω_k is the frequency vector. For the determination of main frequencies meaning periodicity of the system, the power spectrum distribution PSD is used:

$$PSDp(t)(\omega_k) = \|\mathcal{F}p(t)(\omega_k)\|^2 \quad (9)$$

4. RESULTS AND DISCUSSION

4.1. Validation

High frequence pressure measurements were performed in transparent replica without a spray nozzle. The pressure drop signal was recorded for a bed filling of 1 kg particles and a gas volume flow rate of 100 m³/h. The pressure drop signal and the resulting FFT power plot as well as the corresponding data from the simulation are shown in Fig. 2.

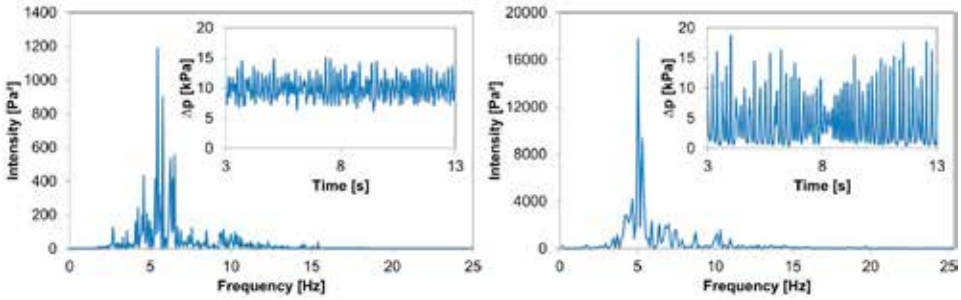

Fig. 2: Pressure drop signal and resulting power plot from experiment (left) and simulation (right); 1 kg γ-Al_2O_3, 100 m³/h.

The pressure fluctuations and the respective power plots show high agreement. The main frequency is in both the experiment and the simulation around 5.5 Hz and also the peak distribution looks similar in both cases. Deviations in amplitudes of pressure signal can be explained by different sampling frequencies and inertia of pressure sensor. It is assumed that the agreement between experiments and simulations is also valid in case of the presence of a nozzle.

4.2. Spray pattern

In order to calibrate the mesh around the nozzle, a spray experiment with dye was performed. A piece of tulle was fixed in the process chamber at a defined height. The fluidization gas was turned on without any particles in the bed. Water with methylene blue was injected at a pump rate of 5 g/min for around 20 seconds. After that time, the process was stopped and the tulle with the blue color on it was pressed on a white sheet of paper. The procedure was repeated at different heights. By means of the different spray pattern prints, the height-dependent area of liquid injection was determined as shown in Fig. 3 and used for the mesh construction of spray zone in the simulations.

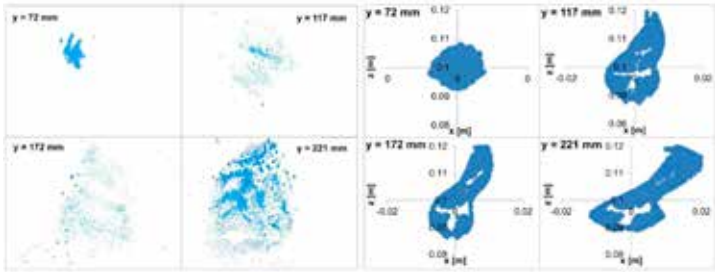

Fig. 3: Experimentally determined spray pattern of two-fluid nozzle (970-S4, Schlick) at different heights and respective constructed nozzle meshes.

4.3. Spouting stability and its improvement

By performing simulations with a bed filling of 1 kg for different gas flow rates, the different flow regimes (fixed bed, bubbling, stable spouting, instable region) were determined. At gas flow rates below 30 m³/h the bed remains constant. With increasing gas velocity bubbles are formed that ascend through the bed to the surface. At gas flow rates between 40 and 70 m³/h stable spouting occurs with the typical areas of spout, fountain and annulus, which can be seen by the slim peak at the characteristic pressure drop frequency in the FFT plot. Exemplarily, snapshots of experimentally observed flow pattern and the respective pressure signals for a gas flow rate of 50 m³/h are shown in Fig. 4.

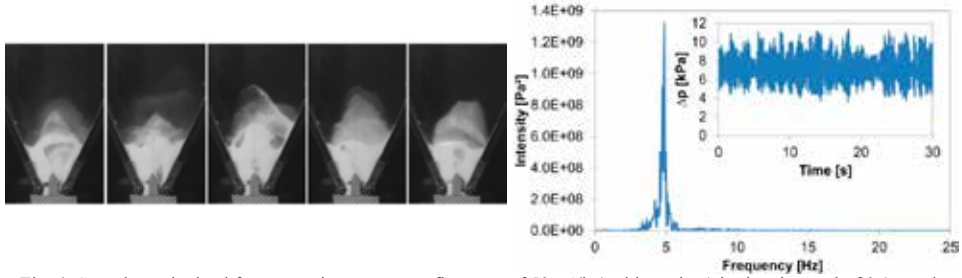

Fig. 4: Snapshots obtained from experiment at a gas flow rate of 50 m³/h (stable regime) in time interval of 0.1 s and corresponding experimentally obtained pressure drop signal with FFT power plot.

At gas flow rates exceeding 70 m³/h, the spouting becomes instable, which can be seen in lateral spout deflections and variations of the bed expansion. The pressure drop fluctuations become more irregular which results in a broader distribution in the power plot. As described by Salikov et al. [5] for pseudo two-dimensional prismatic spouted beds, the region of stable spouting can be increased by inserting draft plates into the process chamber which assist the spouting flow pattern. By running several simulations with different configurations, two parallel plates (60 mm x 10 mm x 20 mm) with a horizontal distance of 45 mm and a distance in vertical direction from middle profile of 10 mm were found to improve best the spouting stability of the regarded ProCell 5 apparatus. Fig. 5 gives a snapshot of the flow pattern as well as the pressure fluctuations and the FFT plots of both configurations that were received by the simulations. As can be seen, the spouting stability is not only qualitatitvely but also quantitatively improved.

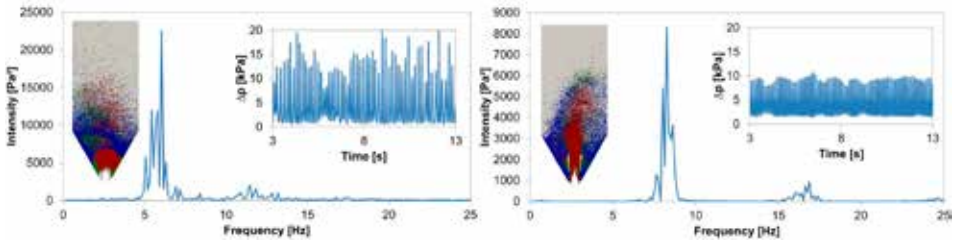

Fig. 5: Snapshots of flow pattern and corresponding pressure drop signal with FFT power plot obtained by simulations for original apparatus (left) and process chamber with draft plates (right).

4.4. Liquid injection

Coating liquid was injected with a rate of 5 g/min. Simulations were performed with different gas volume flow rates. Volume flow rates of 70 m³/h (stable regime), 100 m³/h and 120 m³/h (instable regime) were chosen, whereby the highest flow rate was analysed with and without draft plates. The resulting cumulative number distributions of particles' surface coverage for a process duration of 10 s are shown in Fig. 6. It can be seen that the differences in the distribution are small for the three different flow rates but the curve of the case with draft plates is different. After 10 s, there are more particles that are almost uncoated in case of optimized chamber (≈ 58 %) compared to original geometry (≈ 31 %) but after the intersection of the curves at around 1 % surface coverage, the trend changes, which indicates more particles with higher surface coverages in case of optimized chamber. This phenomenon can be explained by the reduced circulation frequency in the optmized chamber, which results in a longer residence time of particles in the spray zone and thereby a higher liquid loading but at the same time a longer residence time in the annulus zone where no mass transfer takes place. This effect is most dominant in the first seconds of liquid injection as particles in the annulus zone do not get into contact with droplets, which results in a high amount of uncoated particles at that time. In order to exclude this start-up effects, simulations longer than 10 s have to be performed. For coating purposes it is important that the liquid is not sprayed on the plates and that no sticking of particles on the plates occurs. Therefore, experiments with injection of water with methylene blue and a particle bed of 1 kg in the apparatus with inserted draft plates were performed. No sticking of particles occurred and no droplets settled on the draft plates. Thus we conclude that the draft plates do not interfere with the liquid injection and are a promising tool for coating purposes due to the stabilized spouting and droplet capture behavior.

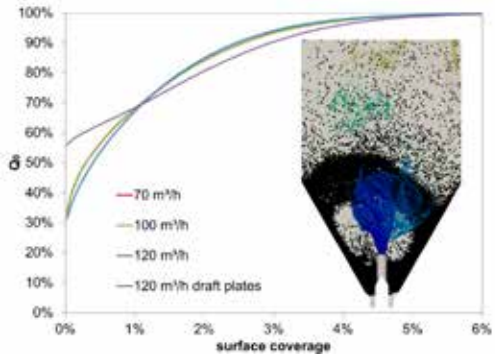

Fig. 6: Cumulative number distribution of particle surface coverage after 10 s and snapshot of liquid droplet injection.

5. CONCLUSIONS

In this contribution, the gas-solid hydrodynamics in a three-dimensional prismatic spouted bed was analyzed by visual observations and by means of pressure drop analysis. The spouting stability was improved by inserting draft plats into the process chamber. As the device is used for coating purposes, the region of liquid injection was determined with dye experiments. The process was modeled with CFD-DEM approach whereby the liquid phase was added in post-processing step. It was found that the influence of the gas volume flow rate on the liquid surface coverage of particles is small but that the draft plates promote higher particle loadings which might be due to the increased residence time of particles in the spray zone.

6. NOTATION

Roman letters

d_d	droplet diameter, m	m	mass, kg
d_p	particle diameter, m	$\boldsymbol{M}_i$	torque, Nm
$\mathcal{F}$	Fourier transformation, -	p	pressure, Pa
$\boldsymbol{F}_d$	drag force, N	N	Number, -
$\boldsymbol{F}_i$	force, N	$\boldsymbol{R}_{pf}$	momentum exchange between particles and fluid, kg·s/m³
$\boldsymbol{g}$	gravitational acceleration, m²/s	S_p	Parcel surface, m²
h	slit height, m	t	time, s
I_i	inertia tensor, kg·m²/rad	Δt	time step, s
K_{pf}	momentum exchange coefficient, -	u	frequency variable, 1/s

$\boldsymbol{u}_f$	fluid velocity, m/s
$\boldsymbol{u}_p$	particle velocity, m/s
$\dot{V}$	fluid volume flow rate, m³/s
V_{cell}	cell volume, m³

Greek letters

α_f	fluid void fraction, -
δ	coarse-graining scaling factor, -
ϑ	Poisson ratio, -
$\eta_{coverage}$	surface coverage, %
μ_f	dynamic viscosity of the fluid, kg/(m·s)
$\mu_{s,p-w}$	static friction coefficient particles/wall,-
$\boldsymbol{x}_i$	center of mass of component i, m
Δx_i	size of mesh cell, m
Y	Young's modulus, Pa
$\mu_{s,p-p}$	static friction coefficient particles/particles,-
$\mu_{s,p-w}$	static friction coefficient particles/wall,-
ρ_f	fluid density, kg/m³
ρ_s	solid density kg/m³
$\boldsymbol{\tau}$	stress tensor, kg/s²
$\boldsymbol{\omega}_i$	angular velocity, rad/s
ω_k	sampling frequency, 1/s

7. REFERENCES

[1] K.B. Mathur, P.E. Gishler, A technique for contacting gases with coarse solid particles, AIChE J. 1 (2) (1955) 157–164.

[2] N. Epstein, J.R. Grace, Spouted and spout-fluid beds: Fundamentals and applications, Cambridge University Press, Cambridge, New York, 2011.

[3] Z. Chen, C.J. Lim, J.R. Grace, Hydrodynamics of slot-rectangular spouted beds: Effect of slot configuration on the local flow structure, Can. J. Chem. Eng. 86 (3) (2008) 598–604.

[4] V. Salikov, S. Antonyuk, S. Heinrich, V.S. Sutkar, N.G. Deen, J. Kuipers, Characterization and CFD-DEM modelling of a prismatic spouted bed, Powder Technology 270 (2015) 622–636.

[5] V. Salikov, S. Heinrich, S. Antonyuk, V.S. Sutkar, N.G. Deen, J. Kuipers, Investigations on the spouting stability in a prismatic spouted bed and apparatus optimization, Special issue of the 7th World Congress on Particle Technology 26 (3) (2015) 718–733.

[6] L.A.P. Freitas, O.M. Dogan, C.J. Lim, J.R. Grace, D. Bai, Identification of Flow Regimes in Slot-Rectangular Spouted Beds using Pressure Fluctuations, Can. J. Chem. Eng. 82 (1) (2004) 60–73.

[7] E. Piskova, L. Mörl, Characterization of spouted bed regimes using pressure fluctuation signals, Chemical Engineering Science 63 (9) (2008) 2307–2316.

[8] O. Gryczka, S. Heinrich, N.G. Deen, M. van Sint Annaland, J. Kuipers, M. Jacob, L. Mörl, Characterization and CFD-modeling of the hydrodynamics of a prismatic spouted bed apparatus, Chemical Engineering Science 64 (14) (2009) 3352–3375.

[9] C.M. van den Bleek, J.C. Schouten, Deterministic chaos: A new tool in fluidized bed design and operation, The Chemical Engineering Journal and the Biochemical Engineering Journal 53 (1) (1993) 75–87.

[10] D. Gidaspow, R. Bezburuah, J. Ding, Hydrodynamics of circulating fluidized beds: Kinetic theory approach, in: 1991.

[11] V.S. Sutkar, N.G. Deen, A.V. Patil, V. Salikov, S. Antonyuk, S. Heinrich, J. Kuipers, CFD–DEM model for coupled heat and mass transfer in a spout fluidized bed with liquid injection, Chemical Engineering Journal 288 (2016) 185–197.

[12] R. Beetstra, M.A. van der Hoef, J.A.M. Kuipers, Drag force of intermediate Reynolds number flow past mono- and bidisperse arrays of spheres, AIChE J. 53 (2) (2007) 489–501.

[13] N.G. Deen, M. van Sint Annaland, M.A. van der Hoef, J. Kuipers, Review of discrete particle modeling of fluidized beds, Fluidized Bed Applications 62 (1–2) (2007) 28–44.

[14] H. Hertz, Ueber die Berührung fester elastischer Körper, Journal für die reine und angewandte Mathematik 92 (1882) 156–171.

[15] C. Bierwisch, T. Kraft, H. Riedel, M. Moseler, Three-dimensional discrete element models for the granular statics and dynamics of powders in cavity filling, Journal of the Mechanics and Physics of Solids 57 (1) (2009) 10–31.

[16] B. Crüger, V. Salikov, S. Heinrich, S. Antonyuk, V.S. Sutkar, N.G. Deen, J. Kuipers, Coefficient of restitution for particles impacting on wet surfaces: An improved experimental approach, Particuology 25 (2016) 1–9.

[17] W.I. Kariuki, B. Freireich, R.M. Smith, M. Rhodes, K.P. Hapgood, Distribution nucleation: Quantifying liquid distribution on the particle surface using the dimensionless particle coating number, Chemical Engineering Science 92 (2013) 134–145.

[18] J.M. Link, PhD thesis: Development and validation of a discrete particle model of a spout-fluid bed granulator, University of Twente, Enschede, 2006.